Tectonophysics xxx (2016) xxx–xxx

Contents lists available at ScienceDirect

Tectonophysics

journal homepage: www.elsevier.com/locate/tecto

Non-linear critical taper model and determination of accretionary wedge strength

Che-Ming Yang, Jia-Jyun Dong *, Yuan-Lung Hsieh, Hsueh-Hua Liu, Cheng-Lung Liu

Graduate Institute of Applied Geology, National Central University, Taiwan

ARTICLE INFO

Article history:
Received 11 March 2015
Received in revised form 3 March 2016
Accepted 13 April 2016
Available online xxxx

Keywords:
Fold-and-thrust belt
Accretionary wedge
Wedge strength
Critical taper model
Hoek–Brown failure criterion
Heterogeneity

ABSTRACT

The critical taper model has been widely used to evaluate the strength contrast between the wedge and the basal detachment of fold-and-thrust belts and accretionary wedges. However, determination of the strength parameters using the traditional critical taper model, which adopts the Mohr–Coulomb failure criterion, is difficult, if not impossible. In this study, we propose a modified critical taper model that incorporates the non-linear Hoek–Brown failure criterion. The parameters in the proposed critical Hoek–Brown wedge CHBW model can be directly evaluated via field investigations and laboratory tests. Meanwhile, the wedge strength is a function of the wedge thickness, which is oriented from stress non-linearity. The fold-and-thrust belt in western central Taiwan was used as an example to validate the proposed model. The determined wedge strength was 0.86 using a representative wedge thickness of 5.3 km; this was close to the inferred value of 0.6 from the critical taper. Interestingly, a concave topographic relief is predicted as a result of the wedge thickness dependency of the wedge strength, even if the wedge is composed of homogeneous materials and if the strength of the detachment is uniform. This study demonstrates that the influence of wedge strength on the critical taper angle can be quantified by the spatial distribution of strength variables and by the consideration of the wedge thickness dependency of wedge strength.

1. Introduction

The critical taper model (Suppe and Wittke, 1977; Davis et al., 1983; Dahlen et al., 1984; Dahlen, 1990) has been widely adopted to depict the evolution of fold-and-thrust belts and accretionary wedges (e.g., Zhao et al., 1986; Breen, 1987; Behrmann et al., 1988; Dahlen and Barr, 1989; Dahlen, 1990; Lallemand et al., 1994; DeCelles and Mitra, 1995; Braathen et al., 1999; Plesch and Oncken, 1999; Carena et al., 2002; Bilotti and Shaw, 2005; Mourgues and Cobbold, 2006; Wang and Hu, 2006; Wang et al., 2006; Yuan et al., 2015). The fold-and-thrust belt and accretionary wedge (represented by "accretionary wedge" or simply "wedge" in this paper), conceptually, are analogous to a homogeneous wedge of snow or sand in front of a moving bulldozer (Fig. 1). It has been recognized that the shape of the wedge is determined by the strength of the wedge and the basal detachment. This hypothesis has already been validated by sandbox experiments (e.g., Buiter, 2012; Graveleau et al., 2012).

The original wedge theory (Davis et al., 1983; Dahlen, 1990), Suppe (2007) proposed a general form to illustrate the effect of the internal strength of the deforming wedge (W) and the shear strength of the basal detachment (F) on the wedge geometry (critical taper angle, $\alpha+\beta$)

$$\alpha+\beta=\frac{\left(1-\rho_f/\rho\right)\beta+F}{\left(1-\rho_f/\rho\right)+W} \tag{1}$$

where α is the slope of topographic relief, β is the dip of basal detachment, and ρ and ρ_f are the densities of the rocks and fluids, respectively, within the wedge. The value of $(1-\rho_f/\rho)$ is 1 for subaerial wedges and is ~0.6 for submarine wedges (Suppe, 2007).

The critical Coulomb wedge theory (Davis et al., 1983; Dahlen et al., 1984; Dahlen, 1990) can be abbreviated to the CCW theory proposed by Yuan et al. (2015). In this study, the terminology of the CCW theory was slightly modified to the Critical Mohr–Coulomb Wedge (CMCW) theory because a Mohr–Coulomb (MC) failure criterion was adopted within the context of the traditional taper model. Because the MC failure criterion was adopted, the wedge strength (W_{MC}), which replaces W in Eq. (1), and the basal detachment strength F can be expressed as

* Corresponding author at: 300, Jhongda Rd., Jhongli, Taoyuan 32001, Taiwan.
E-mail address: jjdong@geo.ncu.edu.tw (J.-J. Dong).

http://dx.doi.org/10.1016/j.tecto.2016.04.026

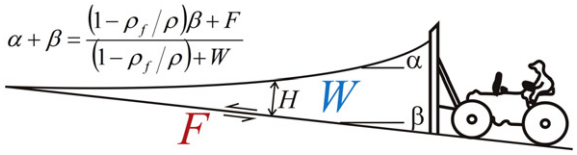

Fig. 1. Schematic diagram of a critical taper model that relates taper angle ($\alpha+\beta$) to the internal and basal strengths of a wedge (modified from Dahlen et al., 1984).

follows

$$W_{MC} = 2(1-\lambda)\left(\frac{\sin\varphi}{1-\sin\varphi}\right) + \frac{C}{\rho g H} \tag{2}$$

$$F = \mu_b(1-\lambda_b) + \frac{C_b}{\rho g H} \tag{3}$$

where g is the gravitational acceleration and H is the wedge thickness, which is measured from the basal detachment to the ground surface and is perpendicular to the basal detachment. φ and μ_b are the friction angle of the wedge and the friction coefficient of the basal detachment, respectively, and C and C_b are the cohesive strength of the wedge and of the basal detachment, respectively. λ and λ_b are, respectively, the Hubbert–Rubey pore-fluid pressure ratios of the wedge and of the basal detachment (Hubbert and Rubey, 1959) and can be expressed as:

$$\lambda = p_f/\sigma_v \tag{4}$$

$$\lambda_b = p_{fb}/\sigma_v \tag{5}$$

where p_f and p_{fb} are the pore-fluid pressures of the wedge and basal detachment, respectively, and σ_v is the vertical stress. The range of λ and λ_b is from 0 (without pore-fluid pressure) to 1 (pore-fluid pressure equal to the vertical stress).

Despite the existence of the CMCW theory, determination of the cohesion (C) and friction angle (φ) of an accretionary wedge is extremely difficult. The C and φ values of intact rock can be obtained from triaxial compressive tests performed in a laboratory. It has been recognized since 19th century, however, that the strength of mountain belts must be less than the strength of intact rocks (Airy, 1855). Presently, the importance of scale effects on the mechanical behaviors of rock masses is well known (e.g., Hudson et al., 1972; Heuze, 1980; Goodman, 1989, Haimson, 1990). Therefore, the laboratory derived C and φ values of intact rocks cannot be used to represent the strength of rock masses in-situ. As such, the knowledge to estimate regional-scale strength parameters is limited. Although crust strength can be inferred from wedge shape (Suppe, 2007) and stress measurements can be inferred from deep boreholes (e.g., Townend and Zoback, 2000), methods for directly evaluating the strength of wedges are unavailable. Additionally, evaluating the heterogeneity of accretionary wedges is also difficult. Aside from these difficulties, the strength non-linearity (i.e., strength will not increase linearly with increasing confining stress) of rock mass is well recognized, and a non-linear Hoek and Brown failure criterion (HB failure criterion) is accordingly proposed (Hoek and Brown, 1980a, 1980b, 1997; Hoek, 1983, 1994; Hoek et al., 1992, 2002). Based on the non-linear HB failure criterion, the apparent friction angle of rock masses could decrease with increasing effective confining stress.

A rock mass classification approach, such as the Rock Mass Rating (*RMR*) system (Bieniawski, 1973, 1989) or the Q system (Barton et al., 1974), is useful for evaluating the strength parameters of rock masses empirically. Based on engineering studies, correlations between strength parameters (e.g., C and φ of the MC failure criterion) and rock mass qualities (e.g., *RMR* and Q values) are available (Bieniawski, 1976, 1989; Mehrotra, 1992; Barton, 2002; Şen and Sadagah, 2003). Hoek (1994) and Hoek et al. (1995) proposed using a Geological Strength Index (*GSI*) to determine the strength parameters of the HB failure criterion. Accordingly, the strength of rock masses can be evaluated directly by field investigation.

This study proposes a modified critical taper model that incorporates the non-linear HB failure criterion. An example of a fold-and-thrust belt in western central Taiwan was used to determine wedge strength based on field investigation. The case study was also used to validate the proposed model. The advantages of the proposed model are noted in comparison to the traditional critical taper model, which adopts an MC failure criterion.

2. Non-linear Hoek–Brown (HB) failure criterion

The HB failure criterion (Hoek and Brown, 1980a, 1980b, 1988; Hoek et al., 1992; Hoek, 1994; Hoek et al., 1995) is recognized by geological/geotechnical engineers worldwide. The original HB failure criterion was developed during the preparation of the book "Underground Excavations in Rock", which was published in 1980 (Hoek and Brown, 1980a). In addition to its non-linear nature, the significance of the HB failure criterion of rock masses lies in its linkage to in-situ geologic characteristics, which initially took the form of Bieniawski's *RMR* and later the *GSI* (Hoek, 1994; Hoek et al., 1995). The *GSI* is an index for directly quantifying rock mass strength that is dependent on rock mass structure and conditions of discontinuity. The *GSI* of a rock mass can be obtained from field investigation. The range of the *GSI* is from 0 to 100, where 0 indicates a rock mass that is highly weathered and laminated/sheared and 100 indicates a rock mass that is fresh and intact/massive.

Since 1980, the HB failure criterion of rock masses was modified several times, and the 2002 edition (Hoek et al., 2002) is a mature version:

$$\sigma^*_{1,f} = \sigma^*_{3,f} + \sigma_{ci}\left(m_b\frac{\sigma^*_{3,f}}{\sigma_{ci}} + s\right)^a \tag{6}$$

where $\sigma^*_{1,f}$ and $\sigma^*_{3,f}$ are the maximum and minimum effective principal stresses at failure, respectively, and σ_{ci} is the uniaxial compressive strength of the intact rock.

In Eq. (6), m_b is a constant related to the lithology and structure of the rock mass, which is given by:

$$m_b = m_i \cdot \exp\left(\frac{GSI-100}{28-14D}\right) \tag{7}$$

where m_i is a material constant that reflects the frictional characteristics of the mineral composition of intact rocks (Hoek and Brown, 1997; Marinos and Hoek, 2001). The m_i chart was established based on numerous triaxial compressive tests for different lithologies. Values for clastic sedimentary rocks are as follows: 4 ± 2 for claystone, 6 ± 2 for shale, 7 ± 2 for siltstone, 17 ± 4 for sandstone, and 21 ± 3 for conglomerate (Marinos and Hoek, 2001).

D is a factor that relates to the disturbance of a rock mass as a result of blasting damage and stress relaxation after engineering excavation. If a rock mass is not affected by the excavation, $D=0$. $D=1$ represents a highly disturbed rock mass due to poor blasting quality. We assume $D=0$ in this study because the engineering disturbance of accretionary wedges is minimized. The influence of geologic structures, such as folding and faulting, is already covered by *GSI*.

The material constants s and a in Eq. (6) can be obtained by the following relationships:

$$s = \exp\left(\frac{GSI-100}{9-3D}\right) \text{ and} \tag{and (8))}$$

$$a = \frac{1}{2} + \frac{1}{6}\left(e^{-GSI/15} - e^{-20/3}\right), \tag{9}$$

Please cite this article as: Yang, C.-M., et al., Non-linear critical taper model and determination of accretionary wedge strength, Tectonophysics (2016), http://dx.doi.org/10.1016/j.tecto.2016.04.026

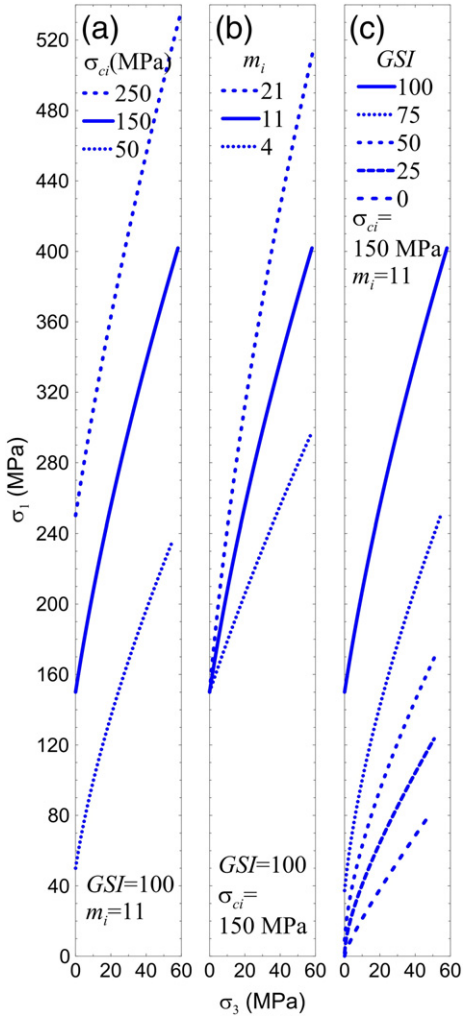

Fig. 2. Failure envelopes of rock masses based on the HB failure criterion. (a) The influence of σ_{ci} when *GSI* equals 100 (intact rocks or fresh, massive rock masses) and m_i equals 11 (mean values of clastic sedimentary rocks). The range of σ_{ci} from 50 to 250 MPa represents a range in rock strength from strong to very strong. (b) The influence of m_i when *GSI* equals 100 and σ_{ci} equals 150 MPa. The range of m_i from 4 to 21 represents the lower and upper bounds of clastic sedimentary rocks. (c) The influence of *GSI* when m_i equals 11 and σ_{ci} equals 150 MPa.

where the ranges of s and a are from 0 to 1 and 0.5–0.67, respectively. $s \cong 0$ and $a \cong 0.67$ represent extremely fractured rock masses ($GSI = 0$) and $s = 1$ and $a = 0.5$ represent intact rocks or massive rock masses ($GSI = 100$).

The failure envelope is a function of *GSI*, σ_{ci}, and m_i with the assumption of $D = 0$. Fig. 2 shows a series of failure envelopes based on the HB failure criterion (Eq. (6)). Fig. 2a, b demonstrate the influence of σ_{ci} and m_i when $GSI = 100$ ($m_b = m_i$, $s = 1$ and $a = 0.5$ based on Eq. (7) through Eq. (9)). The figure shows that for intact rocks or fresh, massive rock masses (where $GSI = 100$), the intercepts of the failure envelope are equal to σ_{ci}. Moreover, the steepness of the failure envelopes is determined by the material constant m_i ($= m_b$). In general, the steepness of failure envelope increases with the increasing m_i.

Fig. 2c shows that the *GSI* significantly influences the shape of the failure envelope. Both the intercept and the steepness of the failure envelope decrease with decreasing *GSI*. The steepness of the failure envelopes is primarily determined by m_b and a, which decrease with decreasing *GSI* (Eqs. (7) and (9)). Meanwhile, the intercept of the failure envelope decreases quickly when *GSI* decreases from 100 to 0. From Eq. (6), $\sigma_{1,f}^{*} = \sigma_{ci}(s)^a$ when $\sigma_{3,f}^{*} = 0$. That is, when s approaches zero ($GSI = 0$), the maximum principal stress will also approach zero ($\sigma_{1,f}^{*} = 0$). Since s is determined by *GSI* (Eq. (8)), the intercept of the failure envelope will be a function of *GSI* and σ_{ci}. Interestingly, Eq. (6) predicts that the uniaxial compression strength will be zero when the rock mass is highly weathered and laminated/sheared ($GSI = 0$).

Notably, the failure envelope could be cut by the tensile strength in the negative minor principal stress axis (Hoek et al., 2002). Since the tension stress is not critical for the consideration of a compressional wedge in this study, only the positive minor principal stresses of the failure envelopes are shown in Fig. 2.

The advantage of the HB failure criterion in comparison to the MC failure criterion primarily lies in its non-linearity. However, the simple MC failure criterion has been widely used, and numerous models require the strength parameters of cohesion and friction angle.

Hoek et al. (2002) presented an approach for obtaining the equivalent cohesion (C') and equivalent friction angle (φ') of the HB failure criterion for rock masses under different confining stresses using a curve fitting technique. The equivalent C' and φ' can be obtained using the following equations:

$$C' = \frac{\sigma_{ci}\left[(1+2a)s + (1-a)m_b\sigma'_{3n}\right](s + m_b\sigma'_{3n})^{a-1}}{(1+a)(2+a)\sqrt{1 + \left(6am_b(s + m_b\sigma'_{3n})^{a-1}\right)/(1+a)(2+a)}} \quad (10)$$

$$\varphi' = \sin^{-1}\left[\frac{6am_b(s + m_b\sigma'_{3n})^{a-1}}{2(1+a)(2+a) + 6am_b(s + m_b\sigma'_{3n})^{a-1}}\right] \quad (11)$$

where

$$\sigma'_{3n} = \sigma'_{3\max}/\sigma_{ci}. \quad (12)$$

$\sigma'_{3\max}$ is the maximum confining stress used to calculate the equivalent C' and φ'. For deep tunnels, $\sigma'_{3\max}$ can be estimated by (Hoek et al., 2002):

$$\frac{\sigma'_{3\max}}{\sigma'_{cm}} = 0.47\left(\frac{\sigma'_{cm}}{\rho g H'}\right)^{-0.94} \quad (13)$$

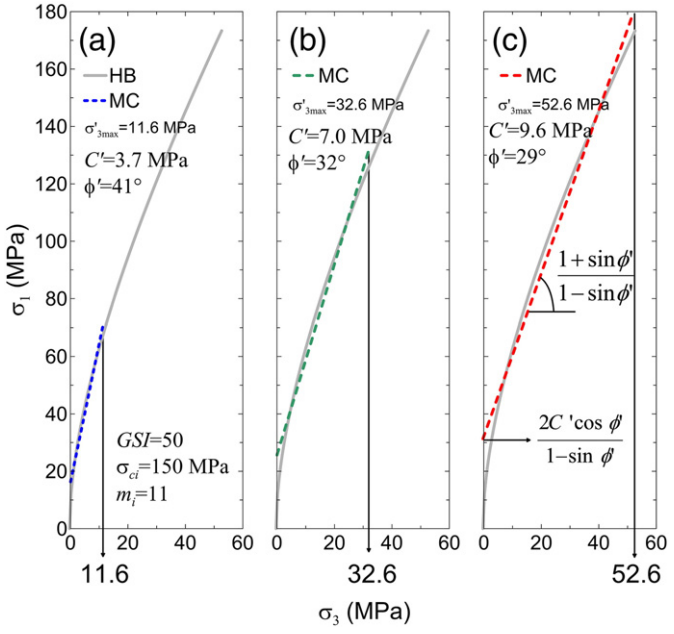

Fig. 3. The HB failure envelope (gray solid line) and the equivalent MC failure envelopes (derived from curve fitting; dashed lines) for a rock mass with *GSI* equal to 50, m_i equal to 11, and σ_{ci} equal to 150 MPa under a $\sigma'_{3\max}$ of (a) 11.6 MPa, (b) 32.6 MPa, and (c) 52.6 MPa.

Please cite this article as: Yang, C.-M., et al., Non-linear critical taper model and determination of accretionary wedge strength, Tectonophysics (2016), http://dx.doi.org/10.1016/j.tecto.2016.04.026

where

$$\sigma'_{cm} = \sigma_{ci}\frac{(m_b + 4s - a(m_b - 8s))((m_b/4) + s)^{a-1}}{2(1+a)(2+a)}. \quad (14)$$

σ'_{cm} is the uniaxial compressive strength of the rock mass (Hoek and Brown, 1997; Hoek et al., 2002). H' is the depth of the tunnel. The equivalent C' and φ' for tunnels at different depths can be computed using a free Windows program called "RocLab," which can be downloaded from www.rocscience.com.

The solid gray curve in Fig. 3 is the HB failure envelope of a rock mass with *GSI* equal to 50, m_i equal to 11, and σ_{ci} equal to 150 MPa. The MC failure criterion in terms of the σ_1^* and σ_3^* can be expressed by

$$\sigma^*_{1,f} = \frac{2C'\cos\varphi'}{1-\sin\varphi'} + \frac{1+\sin\varphi'}{1-\sin\varphi'}\sigma^*_{3,f}, \quad (15)$$

and the failure envelopes are illustrated as dashed lines in Fig. 3 using the calculated equivalent C' and φ' values under different maximum confining stresses (σ'_{3max}). As expected, when a larger maximum confining stress was considered, larger equivalent cohesion values and smaller equivalent friction angles were obtained.

3. Proposed critical taper model incorporating the non-linear HB failure criterion (Critical Hoek–Brown Wedge, CHBW)

The derivation below primarily follows the framework of the critical taper model documented by Davis et al. (1983) and Dahlen (1990). A Cartesian coordinate system (x,z) is employed; x is parallel to the base segment of the wedge between x and $x+dx$, and z increases upward. The thickness of the wedge, measured along the z axis, is denoted by H. For cases of submarine wedges, the water depth, measured along the direction of gravity, is denoted by D_w (Fig. 4). The derivation has two main parts: (1) force equilibrium and (2) full strength mobilization of wedge strength and detachment. That is, the horizontal stress is limited by the wedge strength, and the shear stress on the detachment is equal to the detachment shear strength. The only difference between the traditional critical taper model and the proposed model is that a non-linear failure criterion was used in the derivation to calculate the wedge strength.

The critical taper angle ($\alpha+\beta$) of a horizontally compressed wedge (as shown in Fig. 4) is governed by the force equilibrium of a slice in the x direction. There is a gravitational body force (F_g) whose x component is $-\rho g H dx \sin\beta$, where g is gravitational acceleration and ρ is the saturated rock density. For a submarine wedge, there is a vertical force that results from the water pressure (F_w). The x component is $-\rho_f g D_w \sin(\alpha+\beta)$, where ρ_f is the fluid density. The third force (F_b), which acts on the bottom of the slice, is the frictional resistance to sliding along the basal detachment. In terms of the basal shear traction τ_b, this force is $-\tau_b dx$. The minus sign represents the force acting against the sliding of the wedge. The vertical normal traction σ_{zz} at any point on the wedge is assumed to be solely due to the lithostatic and hydrostatic overburden:

$$\sigma_{zz} = \rho_f g D_w + \rho g(H-z). \quad (16)$$

This assumption is based on a small-angle approximation ($\sin\alpha \approx \alpha$ and $\sin\beta \approx \beta$), which is appropriate given the thin-skinned nature of the wedge. Please note that this assumption will not require if the exact solution of the critical wedge theory (Wang et al., 2006; Yuan et al., 2015) was used to eliminate the induced errors. By defining a dimensionless variable λ, the effective normal traction can be expressed as:

$$\sigma^*_{zz} = (1-\lambda)\rho g(H-z) \quad (17)$$

Thus, the shear traction acting on the base will be

$$\tau_b = \mu_b(1-\lambda_b)\rho g H + C_b \quad (18)$$

if the strength of the detachment is fully mobilized. The fourth force, F_s, is the resultant compressive force of the normal tractions acting on two sides of the slice; a positive value represents compression. Therefore, the force equilibrium satisfies

$$F_g + F_w + F_b = F_s \quad (19)$$

and can be expressed as follows when $dx \to 0$:

$$\rho g H \sin\beta + \rho_f g D_w \sin(\alpha+\beta) + \mu_b(1-\lambda_b)\rho g H + C_b = \frac{d}{dx}\int_0^H \sigma_{xx} dz. \quad (20)$$

Small-angle approximation presumes that $\sin\alpha \approx \alpha$ and $\sin\beta \approx \beta$. With this substitution, Eq. (20) reduces to a simpler form of force equilibrium:

$$\rho g H\beta + \rho_f g D_w(\alpha+\beta) + \mu_b(1-\lambda_b)\rho g H + C_b = \frac{d}{dx}\int_0^H \sigma_{xx} dz. \quad (21)$$

For thin-skinned fold-and-thrust belts and accretionary wedges, the principal stresses are approximately in horizontal and vertical directions, i.e., $\sigma_{3,f} \approx \sigma_{zz}$ and $\sigma_{1,f} \approx \sigma_{xx}$. Eq. (6) can be rewritten as

$$\left(\sigma_{xx} - p_f\right) = \left(\sigma_{zz} - p_f\right) + \sigma_{ci}\left(m_b\frac{\sigma_{zz} - p_f}{\sigma_{ci}} + s\right)^a \quad (22)$$

and can be further reduced to

$$\sigma_{xx} = \sigma_{zz} + \sigma_{ci}\left(m_b\frac{\sigma_{zz} - p_f}{\sigma_{ci}} + s\right)^a. \quad (23)$$

Because

$$\sigma_{zz} = \rho_f g D_w + \rho g(H-z), \quad (24)$$

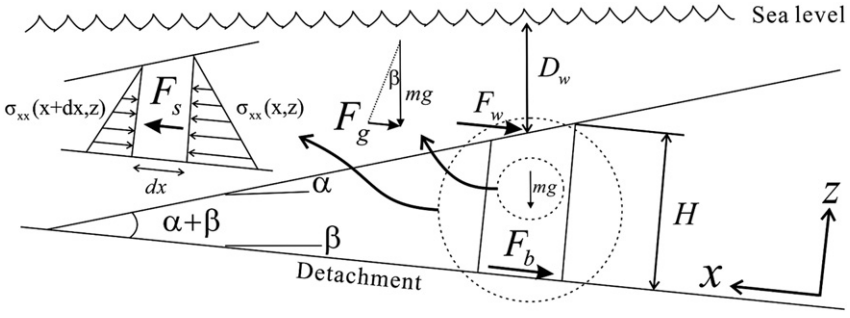

Fig. 4. Schematic diagram of a wedge subjected to horizontal compression (modified from Davis et al., 1983 and Dahlen, 1990). The force equilibrium of a slice (with a width dx) between x and $x+dx$ is shown.

Please cite this article as: Yang, C.-M., et al., Non-linear critical taper model and determination of accretionary wedge strength, Tectonophysics (2016), http://dx.doi.org/10.1016/j.tecto.2016.04.026

Eq. (24) can be rewritten again as

$$\sigma_{xx} = \rho_f g D_w + \rho g(H-z) + \sigma_{ci}\left[m_b\frac{(1-\lambda)\rho g(H-z)}{\sigma_{ci}} + s\right]^a. \quad (25)$$

Inserting Eq. (25) into the integration term of the force equilibrium equation (Eq. (21)), the integration term can be expressed as

$$\int_0^H \sigma_{xx}dz \approx \rho_f g D_w H + \frac{1}{2}\rho g H^2 + \frac{{\sigma_{ci}}^2}{(a+1)m_b(1-\lambda)\rho g} \cdot\left[\frac{m_b\rho gH(1-\lambda)}{\sigma_{ci}} + s\right]^{a+1}\cdot\left[\frac{\sigma_{ci}}{m_b\rho g(1-\lambda)}\right] - \left[\frac{{\sigma_{ci}}^2\cdot s^{a+1}}{(a+1)m_b\rho g(1-\lambda)}\right]. \quad (26)$$

Adopting the small-angle approximation once again, we can obtain $dH/dx = -(\alpha+\beta)$ and $dD_w/dx = \alpha$. Accordingly, the last term in Eq. (21) can be formulated as follows:

$$\frac{d}{dx}\int_0^H \sigma_{xx}dz \approx -\rho_f g D_w(\alpha+\beta) + \rho_f gH\alpha - \rho gH(\alpha+\beta) - (\alpha+\beta)\cdot\sigma_{ci}\left[\frac{m_b(1-\lambda)}{\sigma_{ci}}\rho gH + s\right]^a. \quad (27)$$

Finally, with a substitution of Eq. (27) into Eq. (21), the critical taper angle $\alpha+\beta$ of a wedge can be expressed as

$$\alpha+\beta \approx \frac{\left(1-\rho_f/\rho\right)\beta + \mu_b(1-\lambda_b) + C_b/\rho gH}{\left(1-\rho_f/\rho\right) + \sigma_{ci}\left[\frac{m_b(1-\lambda)}{\sigma_{ci}} + \frac{s}{\rho gH}\right]^a\cdot(\rho gH)^{a-1}}. \quad (28)$$

Subsequently, Eq. (28) can be simplified to

$$\alpha+\beta \approx \frac{\left(1-\rho_f/\rho\right)\beta + F}{\left(1-\rho_f/\rho\right) + W_{HB}} \quad (29)$$

if a non-linear HB failure criterion is adopted.

In Eq. (29), the wedge strength (W_{HB}; assuming the HB failure criterion) is a function of ρ, H, λ, m_b, σ_{ci}, GSI, s and a. The m_b is a function of m_i, GSI, and D (Eq. (7)). The constants s and a are functions of GSI and D (Eqs. (8) and (9)). In this study, the assumption that the disturbance factor D equals zero represents the accretionary wedge has not been disturbed by blasting damage and stress relaxation after engineering excavation. The density of the wedge ρ can be determined precisely, and the variation of the density is relatively low. In total, there are five determining variables that represent the wedge strength W_{HB} in the proposed model: wedge thickness H, Geological Strength Index GSI, uniaxial compressive strength σ_{ci}, material constant m_i, and the Hubbert–Rubey pore-fluid pressure ratio λ. The derived detachment strength F is identical to the original CMCW model (Eq. (3)). The wedge strength of the non-linear CHBW model can be expressed as follows:

$$W_{HB} = \sigma_{ci}\left[\frac{m_b(1-\lambda)}{\sigma_{ci}} + \frac{s}{\rho gH}\right]^a\cdot(\rho gH)^{a-1}. \quad (30)$$

4. Determination of wedge strength using the CHBW model in western central Taiwan

4.1. Study area and geometric parameters

We selected western central Taiwan as an example site to illustrate the features and advantages of the modified critical taper model that incorporates the non-linear HB failure criterion. The study area is shown in Fig. 5. The formations bounded by the Changhua and Chelungpu thrusts are primarily Pleistocene. The outcropped formations range from Pleistocene to Pliocene between the Chelungpu and Shuangtung thrusts, and they primarily range from Miocene to Oligocene–Eocene between the Shuangtung and Tili thrusts. Yue and Suppe (2014) documented a geologic profile (Y-Y′ profile) in the study area. The Y-Y′ profile is shown in Fig. 6. In this study, the Toukoshan Formation between the Changhua and Chelungpu thrusts was divided into two members. The upper, Houyenshan Member (TksHo), primarily consisted of the thick conglomerate layer, while the lower, Hsiangshan Member (ThsHs), consisted of thick sandstone and an interlayer of sandstone and shale (Liu and Lee, 1998). The boundary between TksHo and TksHs is 900 m above the top of the Cholan Formation (Cl), according to Liu and Lee (1998).

The representative slope of topographic relief (α) and the dip angle of basal detachment (β) were determined by Suppe (2007) to be 2° and 2.7°, respectively. The representative thickness of the wedge (H) is 5.3 km. It is a sense of averaged thickness and determined from the wedge thickness at the middle point of the basal detachment (between Changhwa blind thrust and the Tili thrust in Fig. 6). The geometric parameters are shown in Fig. 6. The variables related to wedge strength (GSI,σ_{ci}, and m_i) were obtained from field investigations and laboratory tests, which will be described in the following subsections.

4.2. Determination of GSI values

The wedge strength, given the adoption of the HB failure criterion (W_{HB}), can be calculated by Eq. (28) directly if the necessary parameters are available. To obtain the representative values of GSI for determining the wedge strength, extensive fieldwork was conducted in the study area (Fig. 5). The method used to determine GSI values has been reported in previous publications for different types of rock masses. (Hoek, 1994; Hoek et al., 1995, 1998; Marinos and Hoek, 2000, 2001; Marinos et al., 2005). Tzamos and Sofianos (2007) proposed a quantifiable approach (based on the chart proposed by Sonmez and Ulusay (1999)) to estimate GSI values. The GSI can be determined using following equation:

$$GSI = \left(2.25 + \frac{SR}{120}\right)\cdot SCR + 0.33\cdot SR + 5, \quad (31)$$

where SR is the Structure Rating. SR can be expressed as

$$SR = 79.8 - 17.5\log(J_v). \quad (32)$$

J_v is the volumetric joint count, which is defined as the sum of the number of joints per meter for each joint set (Sonmez and Ulusay, 1999). J_v can be expressed as

$$J_v = \frac{N_x}{L_x}\times\frac{N_y}{L_y}\times\frac{N_z}{L_z}, \quad (33)$$

where N_x, N_y, and N_z are the number of discontinuities counted along the scanlines L_x, L_y, and L_z, which are perpendicular to each other. SCR is the Surface Condition Rating, which can be expressed as

$$SCR = R_r + R_w + R_f, \quad (34)$$

where R_r, R_w, and R_f denote the ratings for roughness, weathering, and infilling of discontinuities, respectively. The ratings follow Table 1, which was proposed by Sonmez and Ulusay (1999).

In total, 110 sites with outcropped Pleistocene to Eocene formations were investigated to evaluate their GSI values based on the method described above. The outcrops of Chinshui Shale (Cs) were always highly slaking. As such, it was difficult to determine the GSI values from outcrop investigation directly. Therefore, this study assumed that Cs belonged to the "E" class ($GSI = 25 \pm 5$), which refers to the specific GSI chart for heterogeneous flysch rock masses (Marinos and Hoek, 2000, 2001). The GSI values of conglomerates were also not obtainable via outcrop investigation using the aforementioned method. Hoek

Please cite this article as: Yang, C.-M., et al., Non-linear critical taper model and determination of accretionary wedge strength, Tectonophysics (2016), http://dx.doi.org/10.1016/j.tecto.2016.04.026

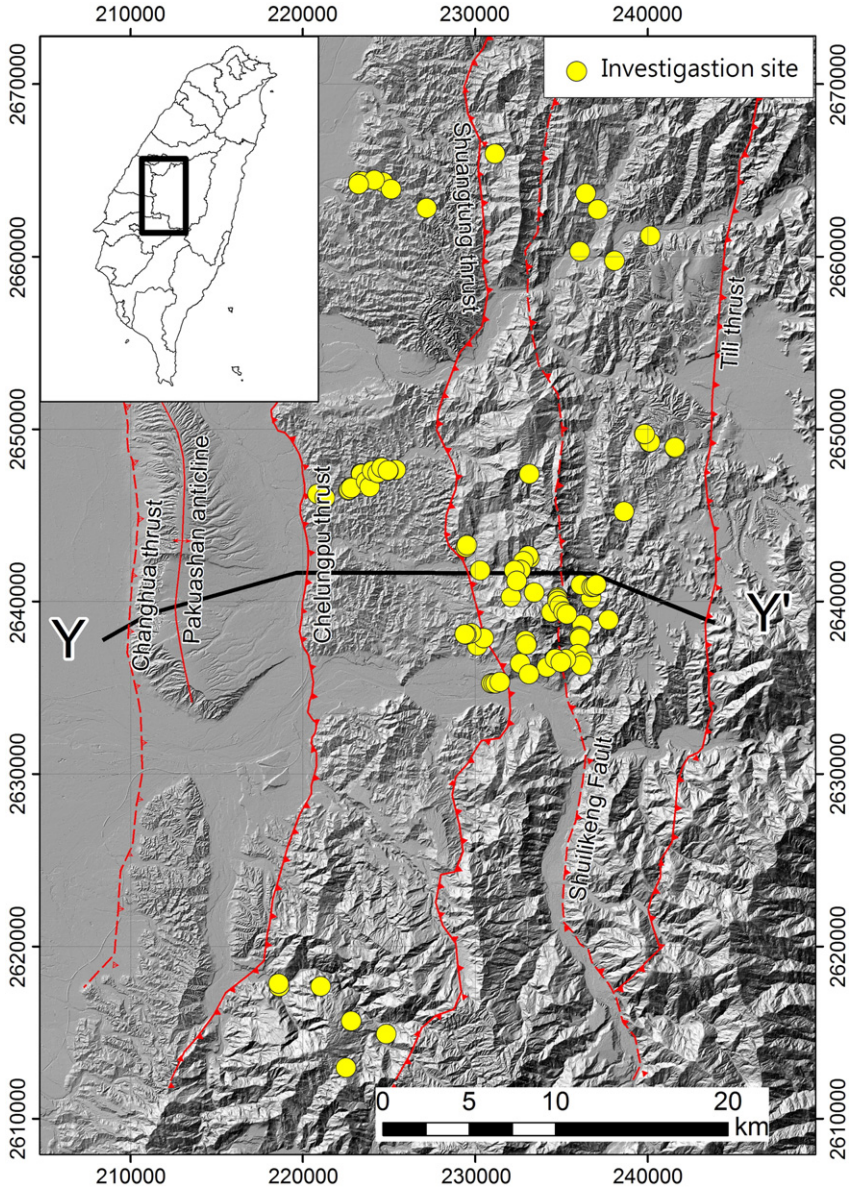

Fig. 5. Study area in western central Taiwan. The locations of the investigation sites for *GSI* evaluations and Schmidt hammer tests are shown as yellow dots. The specimens for point-load tests and uniaxial compressive strength tests were sampled from these investigation sites.

et al. (2005) suggested a specific *GSI* chart for evaluating molasse, which includes conglomerates, sandstones, siltstones, mudstones, and marls. The description of the molasse M3 type was similar to the thickness proportions of TksHo. As such, we assumed a typical range of molasses M3 type ($GSI = 55 \pm 12.5$) to represent the TksHo.

Fig. 7 shows the distribution of the *GSI* values of the formation along the Y-Y′ profile. In general, the mean values of *GSI* ranged from 45 to 65 with the exception of Chinshui Shale (Cs), which was always highly fractured when observed from the Taiwan Chelungpu-fault drilling project (TCDP) hole A (Wu et al., 2008).

4.3. Determination of σ_{ci}

To obtain the representative values of σ_{ci} used to determine wedge strength, extensive field and laboratory work was performed in the study area (Fig. 5). We used the Schmidt hammer test (ASTM, 2005a), the point-load test (ASTM, 2005b), and the uniaxial compressive strength tests (ASTM, 2005c, 2005d) to measure the σ_{ci} of the tested rocks. The Schmidt hammer tests and the point-load tests were conducted in the field, and the uniaxial compressive strength tests were conducted in the laboratory. The specimen preparation and experimental procedure of the uniaxial compressive strength tests were more convenient than the triaxial compressive strength tests. Moreover, the Schmidt hammer tests and point-load tests can be conducted during the field investigation and the test samples can be increased to overcome the representativeness issues.

The results of 104 Schmidt hammer tests, 45 point-load tests, and 103 uniaxial compressive strength tests were used to determine the σ_{ci} of the tested rocks. The determined σ_{ci} was between 3 and 90 MPa. The mean values and the standard deviations of the σ_{ci} of the formations comprising the wedge are shown in Fig. 8. In general, the distribution of σ_{ci} increased from the west (younger formation) to the east (older formation) along the Y-Y′ profile.

As mentioned previously, the Chinshui Shale (Cs) was always highly slaking, and specimens for testing were difficult to obtain from the outcrop. Yeng (2000) documented that the σ_{ci} of Chinshui Shale (Cs) to be 3.2 MPa based on triaxial tests. This reported value was used to represent the σ_{ci} of Cs. It was also difficult to prepare samples of conglomerates to measure the σ_{ci}. Therefore, we used the cohesion and the friction angle from in-situ direct shear tests of the conglomerates to evaluate

Please cite this article as: Yang, C.-M., et al., Non-linear critical taper model and determination of accretionary wedge strength, Tectonophysics (2016), http://dx.doi.org/10.1016/j.tecto.2016.04.026

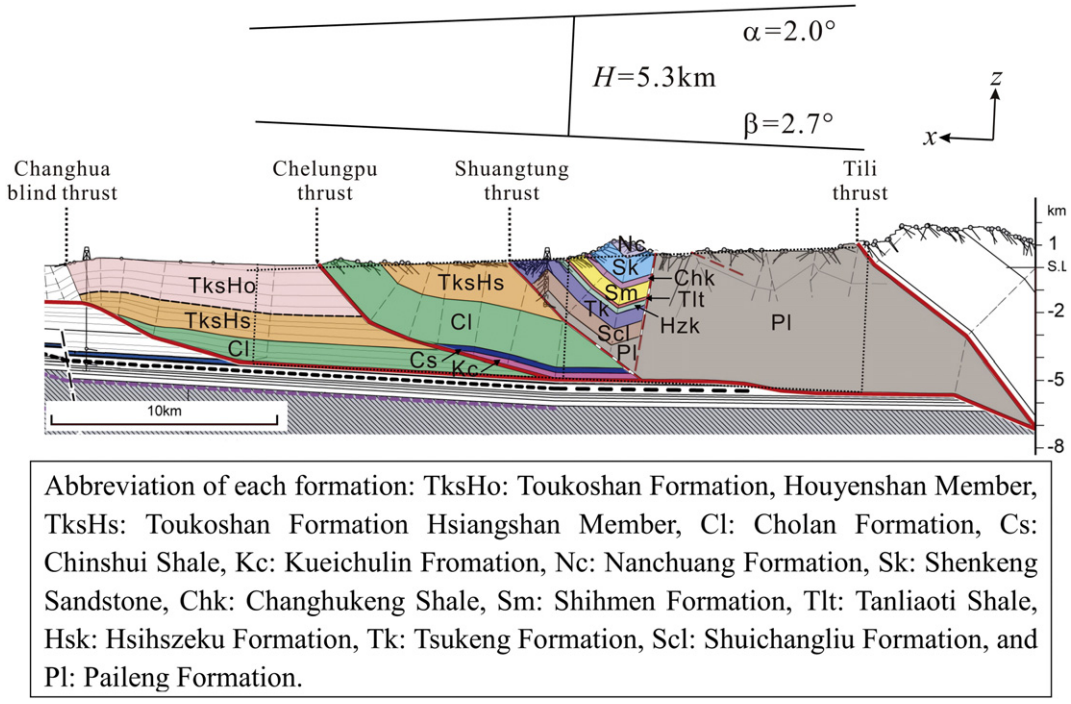

Fig. 6. Y-Y′ profile (modified from Yue and Suppe, 2014). The surface slope (α) and dip angle of basal detachment (β) were determined from Suppe (2007). The representative wedge thickness (H) was measured at the center of this profile.

the σ_{ci} of the Houyenshan Member of the TksHo formation indirectly. The mean and standard deviation of C' and φ' from in-situ direct shear tests under a maximum vertical stress of ~700 kPa were 0.04 ± 0.03 MPa and 38° ± 9°, respectively (Chang et al., 1996; Chu et al., 1996). Using the RocLab software, we determined that $\sigma_{ci} = 3$ MPa corresponded well to the measured C' and φ' given the following inputs: M3 type molasse ($GSI = 55 \pm 12.5$), $m_i = 20.2$ (for TksHo, which will be introduced in Section 4.4), and a maximum vertical stress of ~700 kPa. Therefore, $\sigma_{ci} = 3$ MPa was selected to represent the uniaxial compressive strength of TksHo Formations.

4.4. Determination of m_i

Hoek and Brown (1988) proposed the m_i values for different rock types based on triaxial tests of core samples. The m_i of shale, siltstone, sandstone and conglomerate are 6 ± 2, 7 ± 2, 17 ± 4, 21 ± 3, respectively (Marinos and Hoek, 2001). Along the Y-Y′ profile, the relevant formations frequently consisted of interbedded conglomerate, sandstone, siltstone, and shale. An averaging algorithm was required.

Marinos and Hoek (2001) proposed a chart for determining the flysch types that was related to the lithology, layer thickness proportion, structure, and surface condition. A weighted average table for determining the m_i of different flysch types was suggested. There is not, however, a quantitative standard to categorize flysch type. In this study, we simply used the thickness proportion of each lithology to obtain the weighted average m_i of each formation. Song et al. (2007) provided detail borehole logging of TCDP hole A, which the thicknesses of sandstone, siltstone, and shale is used to determine the m_i of Cs and Kc, respectively. Chen et al. (2001) presented the log of measured Tsaohuchi stratigraphic section in western central Taiwan. The sandstone and shale thicknesses of TksHo, TksHs, and Cl can be obtained from the documented log to determine m_i. The required thickness proportions of sandstone and shale for calculating the weighted average m_i of formations Nc, Sk, Chk, Sm, Tlt, Hzk, Tk, Scl, and Pl are estimated from the qualitative lithologic description of the (Huang et al., 2000). With given thicknesses of (1) massive sandstone, (2) sandstone predominates with minor shale, (3) sandstone and shale interbedded, (4) shale predominates with minor sandstone, and (5) massive shale, the thicknesses proportion of sandstone and shale for specific formation can be calculated using the thickness proportion of each category. The sandstone/shale thickness proportions of the aforementioned five categories are as follows: category (1) sandstone 100% and shale 0%, category (2) 75% sandstone and 25% shale, category (3) 50% sandstone and 50% shale, category (4) 25% sandstone and 75% shale, category (5) 0% sandstone and 100% shale. The proportions of lithological thicknesses and the weighted average m_i of each formation are listed in Table 2.

Table 1
Ratings of R_r, R_w and R_f (proposed by Sonmez and Ulusay, 1999).

Roughness Rating (R_r)	Very rough	Rough	Slightly rough	Smooth	Slikensided
	6	5	3	1	0
Weathering Rating (R_w)	None	Slightly weathered	Moderately weathered	Highly weathered	Decomposed
	6	5	3	1	0
Infilling Rating (R_f)	None	Hard <5 mm	Hard >5 mm	Soft <5 mm	Soft >5 mm
	6	4	2	2	0

4.5. Determination of the wedge strength

Based on the mean values of the evaluated parameters of each formation listed in Table 2, we determined the representative GSI, σ_{ci}, and m_i values of the studied wedge (Y-Y′ profile, Fig. 6) using the proportional area of each formation as a weighting factor. The proportional areas of the formations of concern are listed in Table 2. The calculated representative GSI, σ_{ci}, and m_i values of the Y-Y′ profile in western central Taiwan were 56, 54 MPa, and 14.2, respectively. According to Eq. (7) through Eq. (9), the representative values of GSI, σ_{ci}, and m_i were calculated to be 2.9, 0.007, and 0.504 for the studied wedge. Yue and Suppe (2014) determined that the λ above the basal detachment of the Y-Y′ profile was hydrostatic ($\lambda = 0.4$). The average thickness of the wedge (H) was 5.3 km (Fig. 6) and $\rho = 2500$ kg/m^3 (Davis et al., 1983;

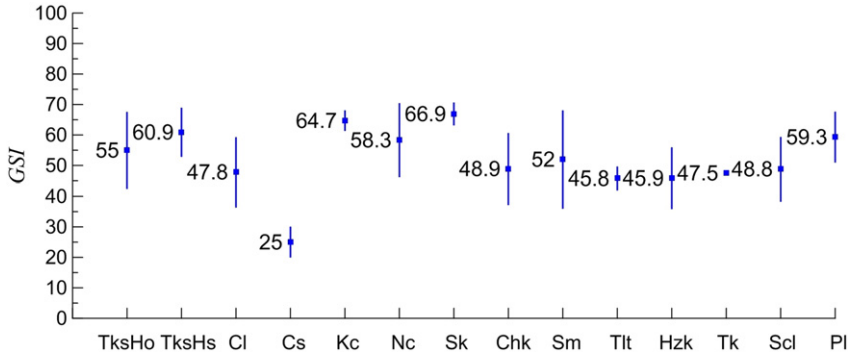

Fig. 7. Means and standard deviations of *GSI* values of the studied formations. The abbreviations of formations are defined in Fig. 6.

Dahlen et al., 1984; Dahlen and Barr, 1989). Therefore, the W_{HB} of the studied wedge (Y-Y′ profile) can be calculated as 0.86 using Eq. (30).

4.6. Validation of the proposed model to estimate the wedge strength

Using the critical taper model that incorporates the non-linear HB failure criterion, the wedge strength for the study area in western central Taiwan was calculated to be 0.86 given an average wedge thickness of 5.3 km. This value was solely determined from direct field and laboratory work. To our knowledge, there is no direct measurement of the strength in the scale of accretionary wedge. To validate the proposed model, the inferred wedge strengths calculated using different approaches in different areas (documented by Suppe (2007)) were compared to the determined wedge strength in the present study. Using the wedge geometry (Carena et al., 2002; Bilotti and Shaw, 2005) to constrain the regional-scale strength without presuming a failure criterion, Suppe (2007) reported that the wedge strengths of the Taiwan and Niger deltas were 0.6 and 0.7, respectively.

Hickman and Zoback (2004) documented the measured maximum and minimum principal stresses in the San Andreas Fault Observatory at Depth (SAFOD) pilot hole. Assuming the stress states at five different depths are at margins of failure and a MC failure criterion was adopted, the cohesion and friction angle can be obtained as 2.3 MPa and 27.3° (Fig. 9). Based on the CMCW model, the wedge strength can be obtained from Eq. (2). The evaluated wedge strength of SAFOD pilot hole is illustrated in Fig. 10. The documented wedge strength was 1.06–1.09 at a depth of 1–2 km. Please note, Suppe (2007) documented the non-cohesive wedge strength of SAFOD pilot hole is about 0.5.

Brudy et al. (1997) documented the principal stresses from 1 km to 8 km in the German Continental Deep Drilling Program in German (KTB). Assuming the stress states are at margins of failure and a MC failure criterion was adopted, Suppe (2007) calculated the wedge strength of the KTB borehole equal 1.0 ± 0.2 (Fig. 10) using the following equation:

$$W = \frac{\sigma_1 - \sigma_3}{\sigma_3} \tag{35}$$

Byerlee (1978) presented the failure criterion of rocks from numerous triaxial tests. Accordingly, the friction coefficient of rocks is 0.85 ($\varphi = 40.4°$) when normal stress is less than 200 MPa. By substituting $\varphi = 40.4°$ and $C = 0$ MPa into Eq. (2) and assuming hydrostatic condition, a wedge strength of 2.2 is obtained.

The determined W_{HB} (0.86) of the Y-Y′ profile is slightly higher than the inferred wedge strength of the active Taiwan mountain belt (wedge strength equal to 0.6) and close to the wedge strength of the Niger delta (wedge strength equal to 0.7). Generally, the determined strength falls within the range of documented strengths of wedges or crust shown in Table 3.

It is important to have added the influence of variability of parameters due to the result on W_{HB} cannot be deterministic but must be presented with a maximum value and a minimum value. To test the influence of the variability of determined parameters on the evaluation of wedge strength, the mean values of *GSI* and σ_{ci} plus and minus one standard deviation of each formation (Table 2) were used to determine the weighted parameters. The weighted parameters plus one standard deviation were $GSI^+ = 65$ and $\sigma_{ci}^+ = 71$ MPa. The weighted parameter minus one standard deviation were $GSI^- = 46$ and $\sigma_{ci}^- = 36$ MPa. The determined W_{HB}^+ using GSI^+ and σ_{ci}^+ was 1.16. The determined W_{HB}^- using GSI^- and σ_{ci}^- was 0.60; a wedge thickness of 5.3 km was used and a hydrostatic condition was assumed. The values of the wedge strength that were calculated taking parameter uncertainty into consideration were still well within the inferred strengths of wedges and crust listed in Table 3.

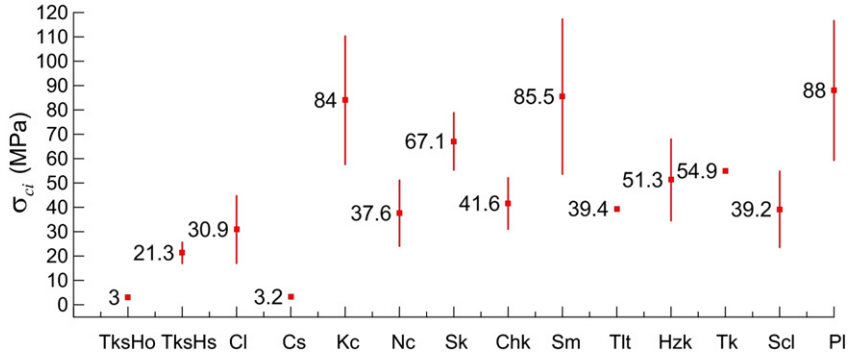

Fig. 8. The means and standard deviations of the σ_{ci} values of the studied formations. The formation abbreviations are defined in Fig. 6.

Please cite this article as: Yang, C.-M., et al., Non-linear critical taper model and determination of accretionary wedge strength, Tectonophysics (2016), http://dx.doi.org/10.1016/j.tecto.2016.04.026

Table 2
The parameters of the HB failure criterion for the studied formations as determined by outcrop investigation with the exception of TksHo and Cs Formations. Weighting is based on the proportional area of a given formation as calculated from the Y-Y′ profile (Fig. 6). The mean value, standard deviation (S.D.) and sample size (n) of *GSI* and σ_{ci} are listed. The formation abbreviations are defined in Fig. 6.

Formation	Weighting	*GSI* ± S.D. (n)	σ_{ci} (MPa) ± S.D. (n)	m_i	Proportions of lithological thicknesses
TksHo	0.100	55 ± 12.5 (−)	3 (−)	20.2	Conglomerate: 79% Sandstone: 21%
TksHs	0.155	60.9 ± 8 (17)	21.3 ± 4.5 (12)	17.2	Conglomerate: 5% Sandstone: 95%
Cl	0.198	47.8 ± 11.4 (13)	30.9 ± 14 (9)	14.3	Sandstone: 76% Shale: 24%
Cs	0.011	25 ± 5 (−)	3.2 (−)	9.7	Sandstone: 27% Siltstone: 72% Shale: 1%
Kc	0.011	64.7 ± 3.3 (6)	84 ± 26.5 (15)	16.4	Sandstone: 94% Siltstone: 4% Shale: 2%
Nc	0.003	58.3 ± 12.1 (8)	37.6 ± 13.7 (5)	13.4	Sandstone: 67% Shale: 33%
Sk	0.015	66.9 ± 3.7 (9)	67.1 ± 11.9 (13)	14.3	Sandstone: 75% Shale: 25%
Chk	0.005	48.9 ± 11.7 (5)	41.6 ± 10.7 (7)	8.8	Sandstone: 25% Shale: 75%
Sm	0.013	52 ± 16 (5)	85.5 ± 32 (4)	9.8	Sandstone: 35% Shale: 65%
Tlt	0.003	45.8 ± 3.8 (6)	39.4 (3)[a]	9.7	Sandstone: 33% Shale: 67%
Hzk	0.006	45.9 ± 10 (11)	51.3 ± 16.9 (10)	11	Sandstone: 46% Shale: 54%
Tk	0.023	47.5 (2)[a]	54.9 (3)[a]	10.3	Sandstone: 39% Shale: 61%
Scl	0.021	48.8 ± 10.5 (12)	37.1 ± 15.8 (8)	7.5	Sandstone: 75% Siltstone: 12.5% Shale: 12.5%
Pl	0.436	59.3 ± 8.3 (14)	88 ± 28.8 (14)	12.5	Sandstone: 59% Shale: 41%

[a] The sample numbers is not sufficient to obtain the standard deviation.

The wedge strength in the proposed CHBW model is confining stress dependent. That is, the wedge strength is a function of the wedge thickness (Eq. (30)). The wedge strengths under different wedge thicknesses (1 km to 8 km) were evaluated and are illustrated in Fig. 10. The W_{HB} decreases from 1.97 to 0.70 when the wedge thickness H increases from 1 km to 8 km (blue line in Fig. 10). The W_{HB} approaches the strength of the Taiwan mountain belt that was inferred by Suppe (2007) at a depth of 8 km. When the wedge thickness decreases, the wedge strength tends to approach the wedge strength calculated based on Byerlee's law. In conclusion, the determined wedge strength of the studied accretionary wedge using the proposed CHBW model is reasonable. The comparison between the proposed CHBW model and the traditional CMCW model will be illustrated in the next section. The advantages and limitations of the proposed method for determining the wedge strength will be discussed further.

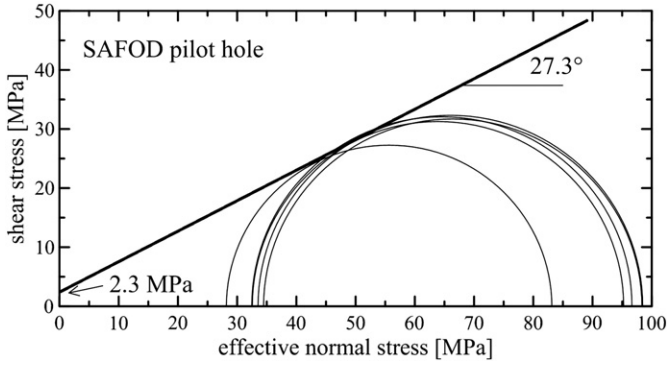

Fig. 9. Five Mohr circles are drawn for the following combinations of maximum and minimum horizontal effective stresses from the SAFOD pilot hole at depth of 1–2 km (data collected from Fig. 4a of Hickman and Zoback (2004)). The failure envelop (solid line) indicated the cohesion and friction angle as 2.3 MPa and 27.3°.

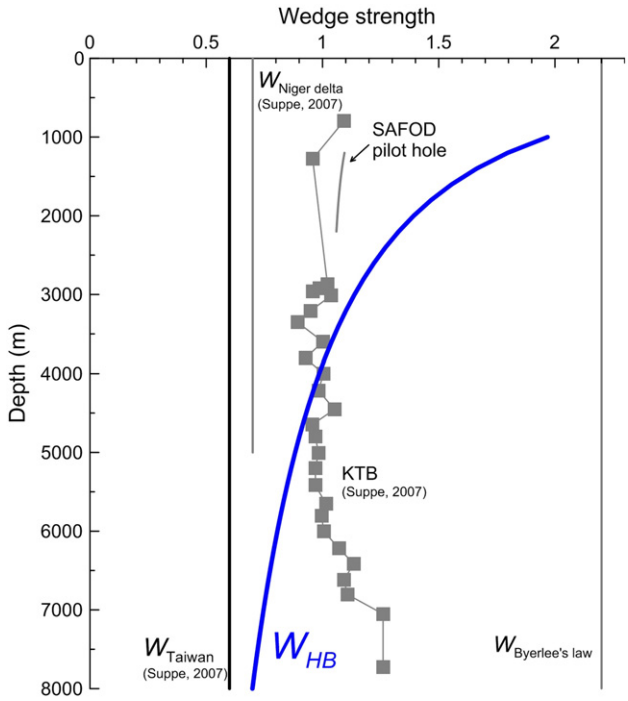

Fig. 10. Wedge strength versus depth. The wedge strength of the Taiwan mountain belt and the Niger delta are shown in addition to borehole stress measurements and the W_{HB} of the Y-Y′ profile (data primarily from Suppe (2007)).

5. Discussion

5.1. The wedge thickness dependency of CHBW and CMCW models

One of the advantages of the CHBW model is that the non-linearity of the strength of the wedge is taken into consideration. Accordingly, the wedge strength can be influenced by the wedge thickness. The traditional CMCW model, however, predicts a dependence of wedge thickness on strength as well (Eq. (2)) if cohesion is not assumed to be zero. To demonstrate the wedge thickness (stress) dependency of the two models, Fig. 11 shows the wedge strengths under a hydrostatic condition as predicted by the HB and MC failure criteria. The equivalent C' and φ' values required to estimate the wedge strength W_{MC} were

Table 3
The comparison of the determined wedge or crust strengths to the inferred strengths documented by Suppe (2007).

	Wedge or crust strengths
California SAFOD pilot hole: at a depth of 1–2 km in granite (Hickman and Zoback, 2004).	1.06 ~ 1.09
Central Taiwan: the depths of cross section 0–15 km (Carena et al., 2002).	0.6
Deep-water thrust belt of the toe of the Niger delta: (Bilotti and Shaw, 2005).	0.7
Western central Taiwan: the representative H is 5.3 km (This study).	0.86
German KTB borehole: to a depth of 8 km (Brudy et al., 1997).	1.0 ± 0.2
Byerlee's law: for rock at normal stress <200 MPa, at a depth of ~13.3 km (Byerlee, 1978).	2.2

Please cite this article as: Yang, C.-M., et al., Non-linear critical taper model and determination of accretionary wedge strength, Tectonophysics (2016), http://dx.doi.org/10.1016/j.tecto.2016.04.026

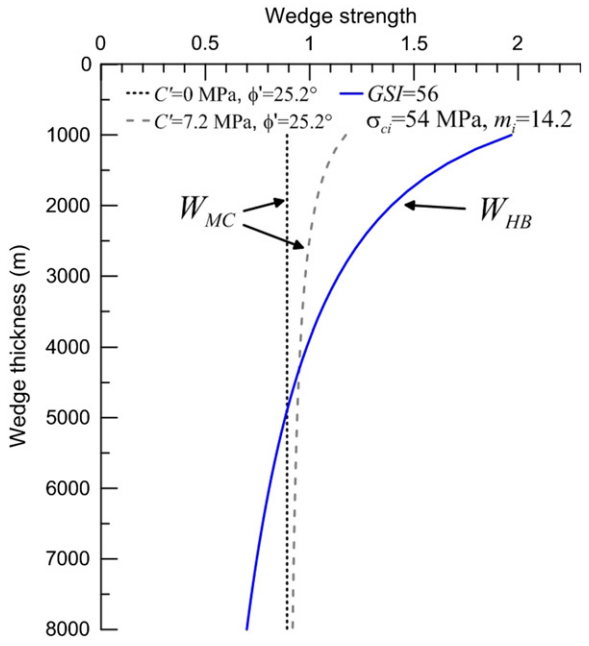

Fig. 11. The wedge thickness dependency of the predicted wedge strength using CHBW and CMCW models.

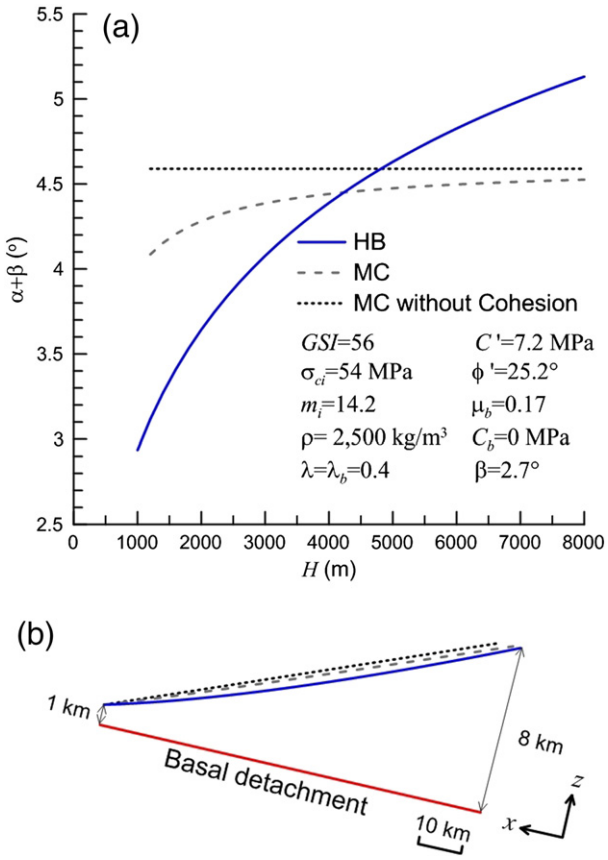

Fig. 12. (a) The calculated $\alpha+\beta$ of CHBW and CMCW models versus the H. (b) The three solutions of Fig. 12(a) are illustrated by the wedge shape in a Cartesian coordinate system (x,z) with $\beta = 2.7°$. The ratio of x to z is 5.

obtained using the method introduced in Chapter 2. A wedge thickness of 8 km was assumed to evaluate the $\sigma'_{3\max}$ to determine the equivalent strength parameters. The horizontal stress at the middle point of the wedge (i.e., 4 km in depth) was used to represent the $\sigma'_{3\max}$ because the maximum principal stress is in horizontal direction. Wu and Dong (2012) suggested that the averaged ratio of the horizontal stress and the vertical stress around the TCDP Borehole was 1.14 based on the results of anelastic strain recovery tests, leak-off tests, borehole breakout, deformation rate analysis, acoustic emission rate analysis, and the acoustic emission method (Lin et al., 2007; Hung et al., 2009; Lin et al., 2010; Yabe et al., 2008). Using Eq. (11) through Eq. (15), the C' and φ' can be determined as 7.2 MPa and 25.2°, respectively, if ρ is assumed to be 2500 kg/m^3 (Dahlen et al., 1984) and λ is assumed to be 0.4.

Fig. 11 shows that the W_{HB} and W_{MC} decreased with increasing H. However, the predicted wedge strength of the CHBW model (W_{HB}) showed a much higher wedge thickness dependency than the one predicted by the CMCW model (W_{MC}). Moreover, as expected (Eq. (2)), the wedge strength predicted using the CMCW model is a constant when the cohesion is assumed to be zero (Fig. 11).

The influence of wedge thickness on the $\alpha+\beta$ for the proposed CHBW model and for the traditional CMCW model was further investigated. The strength parameters used for estimating the wedge strength were identical to the ones used in Fig. 11. The additional required parameters for estimating $\alpha+\beta$ (Eq. (28) and Eq. (1)) are listed in Table 4. Similar to the results shown in Fig. 11, the predicted wedge thickness dependency of $\alpha+\beta$ for the proposed CHBW model is more significant than the dependency predicted by the traditional CMCW model; this is shown in Fig. 12(a). Obviously, this result is a reflection of the non-linearity of wedge strength assumed by adopting the HB failure criterion. Fig. 12(b) shows the wedge shape predicted by the CHBW and CMCW models. If the cohesion of the wedge is zero, the predicted critical taper angle will be a constant. The wedge shape predicted by the CHBW model shows a relatively concave topographic relief (blue solid line in Fig. 12(b)).

Table 4
Geometric parameters and strength variables for the calculation of taper angles.

Variable	Value	Reference
β (°)	2.7	Refer to the study area of the present study in western central Taiwan.
μ_b	0.17	Suppe (2007) suggested that the $F = 0.07$–0.11. If $\mu_b = 0.17$, $C_b = 0$, and $\lambda_b = 0.4$, then $F = 0.1$.
C_b (MPa)	0	C_b is assumed to be 0 MPa.
λ_b	0.4	Assume a hydrostatic condition.
λ	0.4	
ρ (kg/m^3)	2500	Drilling, logging, and core sample data indicate that the mean density of the rocks of the studied wedge is about 2500 kg/m^3 (Dahlen et al., 1984).

5.2. Sensitivity analysis of the strength parameters of HB and MC failure criteria for wedge strength and critical taper angle

The influence of the strength parameters on the predicted wedge strength of the CHBW and CMCW models (Eq. (30) and Eq. (2)) was further investigated. Fig. 13 shows the results of the sensitivity analysis. The base case was $GSI = 50$, $\sigma_{ci} = 150$ MPa, and $m_i = 11$ for the CHBW model, while the base case for the CMCW model was of $C = 10$ MPa and $\varphi = 25°$.

Fig. 13 (a), (b), and (c) demonstrates sensitivity of the wedge strength predicted by the CHBW model (W_{HB}) with respect to strength parameters given wedge thicknesses of 1 km, 3 km, and 5 km, respectively. The horizontal axis shows ±50% variation of the base case parameters ($GSI = 25$–75, $\sigma_{ci} = 75$–225 MPa, and $m_i = 5.5$–16.5). Under the testing conditions, the parameter with the most influence on W_{HB} was GSI. Based on Fig. 13(a), the evaluated wedge strength decreases 40% and increases 65% when GSI decreased or increased by 50%, respectively. The effect of on predicted wedge strength, however the sensitivity of GSI decreased with the increasing H (Fig. 13(a) through Fig. 13(c)). The effects of σ_{ci} and m_i are similar to the effect of GSI; wedge strength decreased 30% and increased 20% given a 50% decrease

Please cite this article as: Yang, C.-M., et al., Non-linear critical taper model and determination of accretionary wedge strength, Tectonophysics (2016), http://dx.doi.org/10.1016/j.tecto.2016.04.026

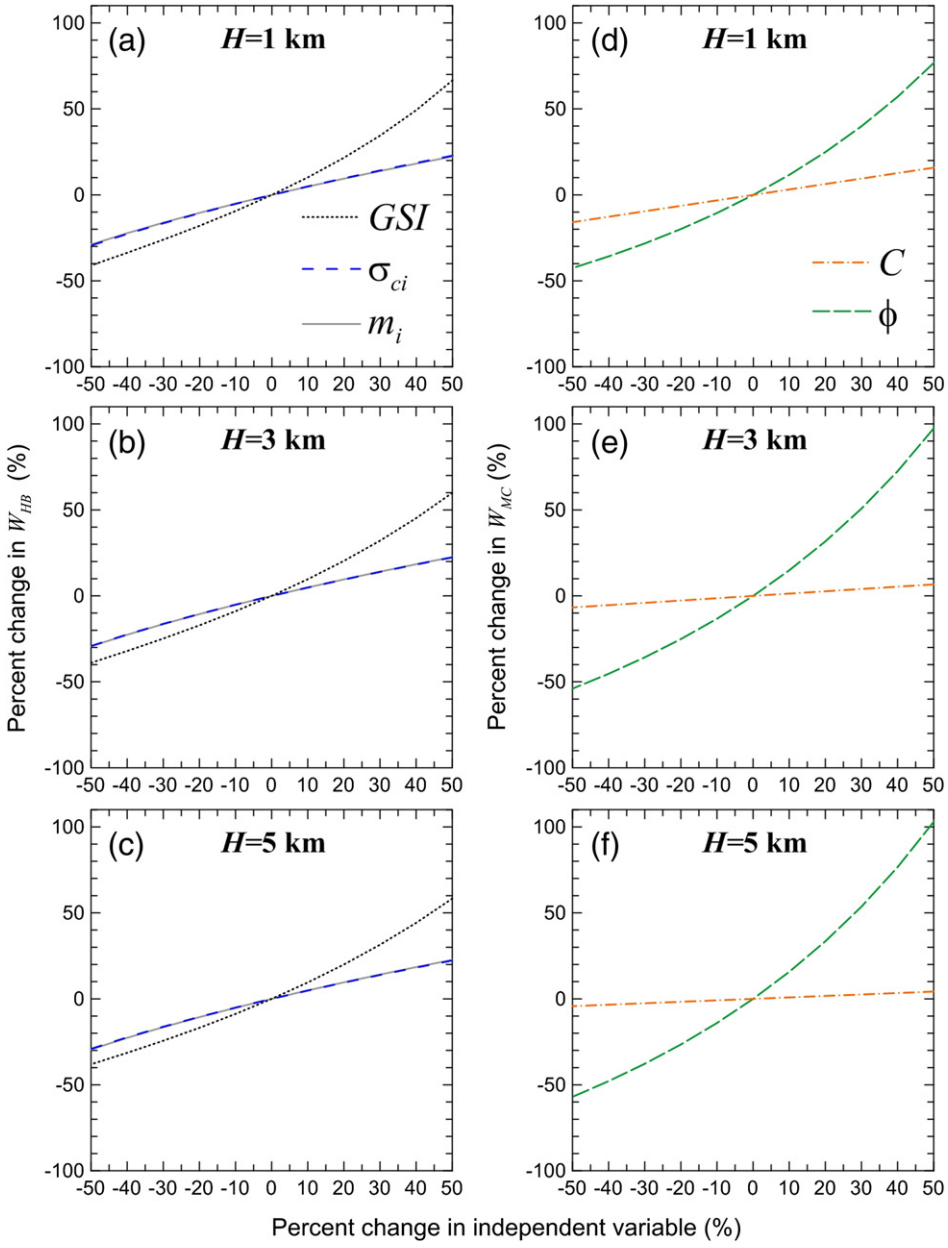

Fig. 13. The sensitivity analysis of wedge strength with respect to the strength parameters. (a)–(c) Effect of parameters on the wedge strength W_{HB} for H equals 1 km, 3 km, and 5 km. (d)–(f) Effect of the parameters on the wedge strength W_{MC} for H equals 1 km, 3 km, and 5 km.

or increase of σ_{ci} and m_i. Furthermore, the influence of wedge thickness H on the sensitivity analysis of σ_{ci} and m_i is insignificant (Fig. 13(a) through Fig. 13(c)).

Fig. 13 (d), (e), and (f) show the effect of C and φ on the predicted values of W_{MC} given a variation of $\pm 50\%$ of the base case parameters. Generally, the effect of φ on wedge strength was larger than the effect of C on wedge strength. A 50% variation of φ induced a 50–90% variation of W_{MC}, but W_{MC} only varied 15% or less when a 50% variation of C was applied.

The effect of the input parameters of CHBW and CMCW models on the critical taper angle $\alpha+\beta$ (Eq. (28) and Eq. (1) can be evaluated based on the results of Fig. 14). The required parameters of Eq. (28) and Eq. (1) are listed in Table 4. Fig. 14(a) shows that a 50% variation of the base case *GSI* (from 25 to 75) results in the variation of $\alpha+\beta$ from -33% to 42% when $H = 1$ km (long dashed lines in Fig. 14(a)). The influence of *GSI* on $\alpha+\beta$ when $H = 5$ km is still substantial (from -38% to 58% variation when a 50% *GSI* variation was applied (Fig. 14(c)). Relatively, the effects of σ_{ci} and m_i on $\alpha+\beta$ are smaller (short dashed lines and solid lines in Fig. 14(a) through Fig. 14(c)). It is reasonable for their insensitivity to the wedge strength (Fig. 13(a) through Fig. 13(c)). These results imply that the determination of *GSI* is critical when a CHBW model is used. Notably, the effect of *GSI* was slightly reduced when the wedge thickness increased.

The effect of φ on $\alpha+\beta$ increased slightly as the wedge thickness increased (Fig. 14(d) through Fig. 14(f)). The importance of φ for predicting $\alpha+\beta$ is greater than that of C under the test conditions. The effect of C on $\alpha+\beta$ was negligible when $H = 5$ km (Fig. 14(f)) because the wedge strength is not influenced by the cohesion (Fig. 13(f)).

5.3. Prospects advantages of the proposed CHBW model

This study proposed a modified critical taper model that incorporated a non-linear HB failure criterion. The most important feature of the proposed CHBW model is the wedge thickness (stress) dependency of the wedge strength W_{HB}. Based on the proposed model, the predicted wedge strength decreases with increasing wedge thickness.

Please cite this article as: Yang, C.-M., et al., Non-linear critical taper model and determination of accretionary wedge strength, Tectonophysics (2016), http://dx.doi.org/10.1016/j.tecto.2016.04.026

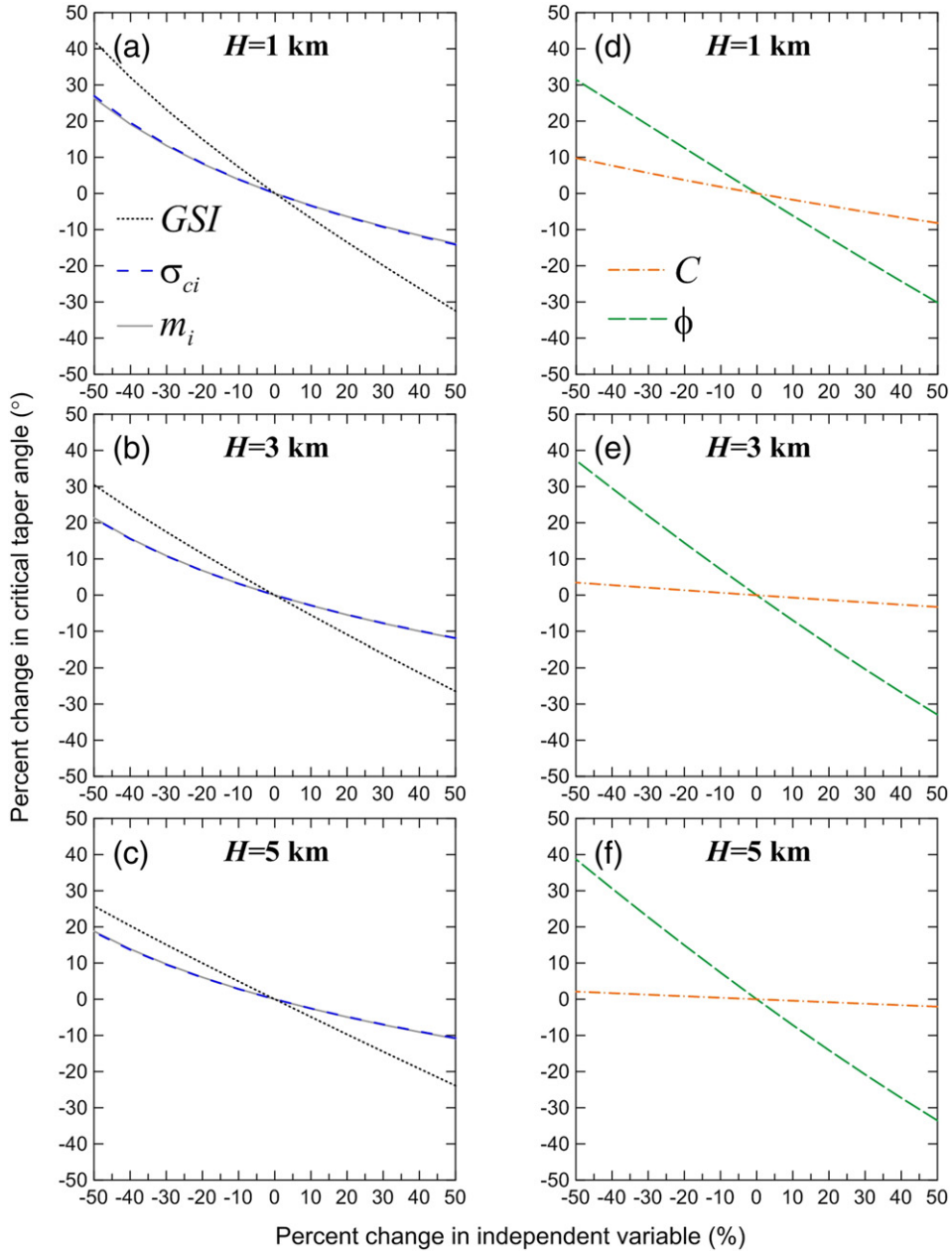

Fig. 14. The sensitivity analysis of the critical taper angle $\alpha+\beta$ with respect to strength parameters. (a), (b), and (c) Effect of parameters on $\alpha+\beta$ for H equals 1 km, 3 km, and 5 km. (d), (e), and (f) Effect of the parameters on $\alpha+\beta$ for H equals 1 km, 3 km, and 5 km.

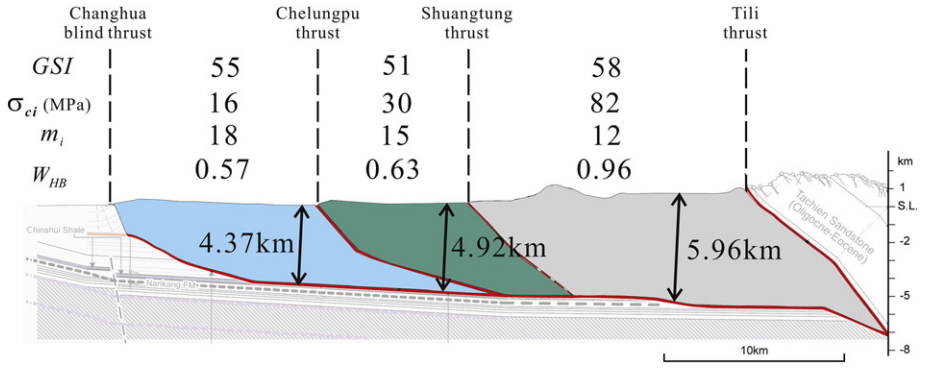

Fig. 15. The Y-Y′ profile was divided into three parts by the Chelungpu thrust and the Shuangtung thrust (modified from Yue and Suppe, 2014). The W_{HB} and the representative strength variables of the three parts are evaluated. The H measured through the center point of each part is measured.

Please cite this article as: Yang, C.-M., et al., Non-linear critical taper model and determination of accretionary wedge strength, Tectonophysics (2016), http://dx.doi.org/10.1016/j.tecto.2016.04.026

Accordingly, the critical taper angle increases with increasing wedge thickness, even when the wedge is composed of homogeneous materials and the strength on the detachment is uniform. That is, evaluation of the determining factors of the concave shape of the wedge ground surface (Flueh et al., 1998) cannot neglect the influence of stress dependency. Indeed, an increased critical taper angle with increasing wedge thickness is also predicted using the traditional CMCW model. However, the trend is much less substantial in comparison to the predicted trend based on the proposed CHBW model (Fig. 12).

In addition to the consideration of stress dependency, we proposed an approach to "measure" the wedge strength. The W_{HB} in the proposed CHBW model can be directly evaluated via field investigations and laboratory tests. Moreover, the heterogeneity of the wedge strength can be evaluated without difficulty. Fig. 7 and Table 2 illustrate the spatial variability of the strength parameters (*GSI*, σ_{ci}, and m_i) of the specific study site. We attempted to demonstrate that the heterogeneity of the wedge strength can be quantified. The Y-Y′ profile was divided into three sub-wedges. The boundaries of these sub-wedges were the Chelungpu thrust and the Shuangtung thrust (Fig. 15). Based on the weighted average parameters listed in Fig. 15, the wedge strength W_{HB} of the three sub-wedges were 0.57, 0.63, and 0.96 from west to east. That is, the evaluated wedge strength along the Y-Y′ profile increased slightly from west to east. It appeared that the strength non-linearity of wedge strength could be compensated for by mechanical heterogeneity based on the Taiwan case. Together with the quantified stress dependency and the heterogeneity of wedge strength, the proposed model could be used to better constrain the detachment strength and the pore pressure heterogeneity based on the measured geometric characteristics of the wedge.

Several limitations related to the use of non-linear HB failure criterion for wedge strength estimation are discussed. First, the HB failure criterion and the method to estimate the strength parameters were established based on engineering experiences. More case studies to validate the appropriateness of using the CHBW model to evaluate the strength of fold-and-thrust belts and accretionary wedges should be undertaken in the future. Second, the site investigation was performed on outcrops while the samples for laboratory tests were from the ground surface. The suitability of the obtained parameters such as *GSI* (different depths could show different geologic structure) and σ_{ci} (weathering effect) to estimate the wedge strength in depth needs further study. The under-sampled shale also presents an issue of representativeness and could result in overestimation of wedge strength. Additionally, the difficulties associated with evaluating strength parameters of conglomerates are also troublesome. Using the charts and tables for determining the strength parameters of flysch and molasse proposed by Hoek et al. (2005) and Marinos and Hoek (2001) is an alternative. The simplification procedure for determining the m_i and *GSI* of interbedded layers of clastic sedimentary rocks is efficient, but the methodology is less quantified compared with the method proposed by Sonmez and Ulusay (1999). The comparison between these two methods for determining the wedge strength is obviously required for further application on critical taper model.

6. Conclusions

The traditional CMCW model frequently assumes that a wedge is mechanically uniform and utilizes cohesion and friction angle, which are difficult to measure, to evaluate wedge strength. This study proposed a modified critical taper model that incorporated a non-linear HB failure criterion to consider the wedge thickness dependency of wedge strength W_{HB}. As such, the W_{HB} predicted by the proposed CHBW model can be directly evaluated via field investigations and laboratory tests. The heterogeneity of the wedge strength can thus be evaluated without difficulties. The accretionary wedge in western central Taiwan was used as an example to validate the proposed CHBW model. The influence of the strength parameters on predicted wedge strength and critical taper angle were also evaluated. The main findings of this study are summarized as follows:

(1) The wedge strength decreases with increasing wedge thickness based on the proposed CHBW model. A concave wedge surface could be related to this wedge thickness dependency. That is, even if the wedge is composed of homogeneous materials and the basal detachment strength and dip are uniform, the critical taper angle will increase with the increasing H because the wedge strength decreased accordingly.
(2) Based on extensive fieldwork and laboratory testing, the *GSI* was between 45 and 65, and the σ_{ci} was between 3 and 90 MPa for the study area. The weighted m_i was between 7.5–20.2, which was primarily determined by the lithology. The determined W_{HB} of the studied Y-Y′ profile was 0.86 when a representative wedge thickness of 5.3 km was used. The determined W_{HB} was slightly higher than the W_{HB} (0.6) suggested by Suppe (2007), which was inferred from the critical taper angle indirectly.
(3) The heterogeneity of an accretionary wedge can be quantified using the spatial variation of the strength variables in the HB failure criterion. The evaluated wedge strength W_{HB} of the three sub-wedges were 0.57, 0.63, and 0.96 from west to east. Together with the stress dependency, the proposed model can be used to better constrain the detachment strength and the pore pressure heterogeneity based on the measured geometric characteristics of the wedge.
(4) The *GSI* is the most dominant parameter in the HB failure criterion for estimating the wedge strength and critical taper angle. Relatively, the effects of σ_{ci} and m_i on the wedge strength and critical taper angle are smaller. That is, accurately determining the *GSI* is critical for application of the proposed model to the study of accretionary wedges.

Acknowledgments

This research was funded by the National Science Council, Taiwan under the grants of NSC 101-2116-M-008-009, 102-2116-M-008-005 and 103-2116-M-008-005. We thank the Editor, Managing Guest Editor of this special issue, Dr. Siame and two anonymous reviewers for their useful and constructive reviews which greatly improved this paper.

References

Airy, G.B., 1855. On the computation of the effect of attraction of mountain-masses, as disturbing the apparent astronomical latitude of stations in geodetic surveys. Philos. Trans. Roy. Soc. London 145, 101–104.
ASTM, 2005a. Standard test method for determination of rock hardness by rebound hammer method. D5873.
ASTM, 2005b. Standard test method for determination of the point load strength index of rock and application to rock strength classifications. D5731.
ASTM, 2005c. Standard practices for preparing rock core as cylindrical test specimens and verifying conformance to dimensional and shape tolerances. D4543.
ASTM, 2005d. Standard test method for unconfined compressive strength of intact rock core specimens. D2938.
Barton, N., Lien, R., Lunde, J., 1974. Engineering classification of rock masses for the design of tunnel support. Rock Mech. 6 (4), 189–236.
Barton, N., 2002. Some new Q-value correlations to assist in site characterization and tunnel design. Int. J. Rock Mech. Min. Sci. 39 (2), 185–216.
Behrmann, J.H., Brown, K., Moore, J.C., Mascle, A., Taylor, E., Alvarez, F., Andreiff, P., Barnes, R., Beck, C., 1988. Evolution of structures and fabrics in the Barbados accretionary prism. Insights from Leg 110 of the Ocean Drilling Program. J. Struct. Geol. 10 (6), 577–591.
Bieniawski, Z.T., 1973. Engineering classification of jointed rock masses. 15. Civil Engineer in South Africa 353-343.
Bieniawski, Z.T., 1976. Rock mass classification in rock engineering. Proc. Symp. Expl. Rock Eng., Johannesburg 1. Balkema, Cape Town, pp. 97–106.
Bieniawski, Z.T., 1989. Engineering rock mass classifications (257 pp).
Bilotti, F., Shaw, J.H., 2005. Deep-water Niger Delta fold and thrust belt modeled as a critical-taper wedge: the influence of elevated basal fluid pressure on structural styles. AAPG Bull. 89 (11), 1475–1491.

Please cite this article as: Yang, C.-M., et al., Non-linear critical taper model and determination of accretionary wedge strength, Tectonophysics (2016), http://dx.doi.org/10.1016/j.tecto.2016.04.026

Braathen, A., Bergh, S.G., Maher, H.D., 1999. Application of a critical wedge taper model to the Tertiary transpressional foldthrust belt on Spitsbergen. Svalbard. Geol. Soc. Am. Bull. 111 (10), 1468–1485.

Breen, N.A., 1987. Three investigations of accretionary wedge deformation: Ph.D. Thesis, University of California — Santa Cruz, Santa Cruz, California, (132 pp).

Brudy, M., Zoback, M.D., Fuchs, K., Rummel, F., Baumgärtner, J., 1997. Estimation of the complete stress tensor to 8 km depth in the KTB scientific drill holes: implications for crustal strength. J. Geophys. Res. 102 (B8), 18453–18475.

Buiter, S.J.H., 2012. A review of brittle compressional wedge models. Tectonophysics 530-531, 1–17.

Byerlee, J.D., 1978. Friction of rocks. Pure Appl. Geophys. 116 (4–5), 615–626.

Carena, S., Suppe, J., Kao, H., 2002. Active detachment of Taiwan illuminated by small earthquakes and its control of first-order topography. Geology 30 (10), 935–938.

Chang, C.T., Chen, Y.J., Yen, S.T., Chai, Y.C.E., 1996. Study of engineering properties and construction method for gravel formations in central and northern Taiwan. Sino-Geotechnics 55, 35–46 (in Chinese).

Chen, W.S., Ridgway, K.D., Horng, C.S., Chen, Y.G., Shea, K.S., Yeh, M.G., 2001. Stratigraphic architecture, magnetostratigraphy, and incised-valley systems of the Pliocene-Pleistocene collisional marine foreland basin of Taiwan: eustatic and tectonic controls on deposition. Geol. Soc. Am. Bull. 113 (10), 1249–1271.

Chu, B.L., Pan, J.M., Chang, K.H., 1996. Field geotechnical engineering properties of gravel formations in western Taiwan. Sino-Geotechnics 55, 47–58 (in Chinese).

Dahlen, F.A., Suppe, J., Davis, D., 1984. Mechanics of fold- and-thrust belt and accretionary wedges: cohesive coulomb theory. J. Geophys. Res. 89, 10087–10101.

Dahlen, F.A., Barr, T.D., 1989. Brittle frictional mountain building: 1. deformation and mechanical energy budget. J. Geophys. Res. 94 (B4), 3906–3922.

Dahlen, F.A., 1990. Critical taper model of fold-and-thrust belts and accretionary wedges. Annu. Rev. Earth Planet. Sci. 18, 55–99.

Davis, D., Suppe, J., Dahlen, F.A., 1983. Mechanics of fold-and-thrust belts and accretionary wedges. J. Geophys. Res. 88 (B2), 1153–1172.

DeCelles, P.G., Mitra, G., 1995. History of the Sevier orogenic wedge in terms of critical taper models, northeast Utah and southwest Wyoming. Geol. Soc. Am. Bull. 107 (4), 454–462.

Flueh, E.R., Fisher, M.A., Bialas, J., Childs, J.R., Klaeschen, D., Kukowski, N., Parsons, T., Scholl, D.W., Brink, Uri ten, Trehu, A.M., Vidal, N., 1998. New seismic images of the Cascadia subduction zone from cruise SO108 — ORWELL, Tectonophysics 293, 69–84.

Goodman, R.E., 1989. Introduction to rock mechanics (476 pp).

Graveleau, F., Malavieille, J., Dominguez, S., 2012. Experimental modelling of orogenic wedges: a review. Tectonophysics 538–540, 1–66.

Haimson, B.C., 1990. Scale effects in rock stress measurements. Proc. Int. Work. Scale Effects Rock Masses 89–101.

Heuze, F.E., 1980. Scale effects in the determination of rock mass strength and deformability. Rock Mech. 12 (3–4), 167–192.

Hickman, S., Zoback, M., 2004. Stress orientations and magnitudes in the SAFOD pilot hole. Geophys. Res. Lett. 31, L15S12. http://dx.doi.org/10.1029/2004GL020043.

Hoek, E., Brown, E.T., 1980a. Underground Excavations in Rock. Institution of Mining and Metallurgy, London (527 pp).

Hoek, E., Brown, E.T., 1980b. Empirical strength criterion for rock masses. J. Geotech. Eng. Div. 106 (GT9), 1013–1035.

Hoek, E., 1983. Strength of jointed rock masses. 23rd. Rankine Lecture. Géotechnique 33 (3), 187–223.

Hoek, E., Brown, E.T., 1988. The Hoek-Brown failure criterion — a 1988 update. Proc. 15th Canadian Rock Mech. Symp. 31–38.

Hoek, E., Wood, D., Shah, S., 1992. A modified Hoek-Brown criterion for jointed rock masses. ISRM Symposium. British Geotechnical Society, London, pp. 209–214.

Hoek, E., 1994. Strength of rock and rock masses. ISRM News J. 2 (2), 4–16.

Hoek, E., Kaiser, P.K., Bawden, W.F., 1995. Support of underground excavations in hard rock. Balkema, Rotterdam.

Hoek, E., Brown, E.T., 1997. Practical estimates of rock mass strength. Int. J. Rock Mech. Min. Sci. Geomech. Abstr. 34 (8), 1165–1186.

Hoek, E., Marinos, P., Benissi, M., 1998. Applicability of the geological strength index (GSI) classification for very weak and sheared rock masses: the case of the Athens schist formation. Bull. Eng. Geol. Env. 57 (2), 151–160.

Hoek, E., Carranza-Torres, C., Corkum, B., 2002. Hoek–Brown failure criterion – 2002 edition. 5th North American rock mechanics symposium and 17th tunnelling association of Canada conference. 1, pp. 267–273.

Hoek, E., Marinos, P.G., Marinos, V.P., 2005. Characterisation and engineering properties of tectonically undisturbed but lithologically varied sedimentary rock masses. Int. J. Rock Mech. Min. Sci. 42 (2), 277–285.

Huang, C.S., Shea, K.S., Chen, M.M., 2000. Explanatory text of the geologic map of Taiwan scale 1:50,000 Sheet 32 PULI. Central Geological Survey, MOEA, Taipei (in Chinese).

Hudson, J.A., Crouch, S.L., Fairhurst, C., 1972. Soft, stiff and servo-controlled testing machines: a review with reference to rock failure. Eng. Geol. 6 (3), 155–189.

Hung, J.H., Ma, K.F., Wang, C.Y., Ito, H., Lin, W., Yeh, E.C., 2009. Subsurface structure, physical properties, fault-zone characteristics and stress state in scientific drill holes of Taiwan Chelungpu Fault Drilling Project. Tectonophysics 446, 307–321.

Hubbert, M.K., Rubey, W.W., 1959. Role of fluid pressure in mechanics of overthrust faulting. 1. mechanics of fluid-filled porous solids and its application to overthrust faulting. Bull. Geol. Soc. Am. 70, 115–166.

Lallemand, S.E., Schnürle, P., Malavieille, J., 1994. Coulomb theory applied to accretionary and nonaccretionary wedges: possible causes for tectonic erosion and/or frontal accretion. J. Geophys. Res. 99 (B6), 12033–12055.

Lin, W., Yeh, E.C., Ito, H., Hirono, T., Soh, W., Wang, C.Y., Ma, K.F., Hung, J.H., Song, S.R., 2007. Preliminary results of stress measurement using drill cores of TCDP Hole-A: an application of an elastic strain recovery method to 3D in-situ stress determination. Terr. Atmos. Ocean. Sci. 18 (2), 379–393.

Lin, W., Yeh, E.C., Hung, J.H., Haimson, B., Hirono, T., 2010. Localized rotation of principal stress around faults and fractures determined from borehole breakouts in hole B of the Taiwan Chelungpu-fault Drilling Project (TCDP). Tectonophysics 482, 82–91.

Liu, H.C., Lee, J.F., 1998. Explanatory text of the geologic map of Taiwan scale 1:50,000 Sheet 38 YUNLIN. Central Geological Survey, MOEA, Taipei (in Chinese).

Marinos, P., Hoek, E., 2000. GSI: a geologically friendly tool for rock mass strength estimation. International conference on geotechnical & geological engineering, Melbourne, pp. 1422–1442.

Marinos, P., Hoek, E., 2001. Estimating the geotechnical properties of heterogeneous rock masses such as flysch. Bull. Eng. Geol. Env. 60 (2), 85–92.

Marinos, V., Marinos, P., Hoek, E., 2005. The geological strength index: applications and limitations. Bull. Eng. Geol. Env. 64, 55–65.

Mehrotra, V.K., 1992. Estimation of engineering parameters of rock mass. IIT Roorkee, Uttarakhand, India (Ph.D. Thesis, 267 pp).

Mourgues, R., Cobbold, P.R., 2006. Thrust wedges and fluid overpressures: sandbox models involving pore fluids. J. Geophys. Res. 111, B05404. http://dx.doi.org/10.1029/2004JB003441.

Plesch, A., Oncken, O., 1999. Orogenic wedge growth during collision — constraints on mechanics of a fossil wedge from its kinematic record (Rhenohercynian FTB, central Europe). Tectonophysics 309, 117–139.

Şen, Z., Sadagah, B.H., 2003. Modified rock mass classification system by continuous rating. Eng. Geol. 67 (3), 269–280.

Song, S.R., Kuo, L.W., Yeh, E.C., Wang, C.Y., Hung, J.H., Ma, K.F., 2007. Characteristics of the lithology, fault-related rocks and fault zone structures in TCDP Hole-A. Terr. Atmos. Ocean. Sci. 18 (2), 243–269.

Sonmez, H., Ulusay, R., 1999. Modifications to the geological strength index (GSI) and their applicability to stability of slopes. Int. J. Rock Mech. Min. Sci. 36 (6), 743–760.

Suppe, J., Wittke, J.H., 1977. Abnormal pore-fluid pressure in relation to stratigraphy and structure in the active fold-and-thrust belt of northwestern Taiwan. Pet. Geol. Taiwan 14, 11–14.

Suppe, J., 2007. Absolute fault and crustal strength from wedge tapers. Geology 35 (12), 1127–1130.

Townend, J., Zoback, M.D., 2000. How faulting keeps the crust strong. Geology 28 (5), 399–402.

Tzamos, S., Sofianos, A.I., 2007. A correlation of four rock mass classification systems through their fabric indices. Int. J. Rock Mech. Min. Sci. 44 (4), 477–495.

Wang, K., Hu, Y., 2006. Accretionary prisms in subduction earthquake cycles: the theory of dynamic Coulomb wedge. J. Geophys. Res. 111, B06410. http://dx.doi.org/10.1029/2005JB004094.

Wang, K., He, J., Hu, Y., 2006. A note on pore fluid pressure ratios in the Coulomb wedge theory. Geophys. Res. Lett. 33, L19310. http://dx.doi.org/10.1029/2006GL027233.

Wu, W.J., Dong, J.J., 2012. Determining the maximum overburden along thrust faults using a porosity versus effective confining pressure curve. Tectonophysics 578, 63–75.

Wu, Y.H., Yeh, E.C., Dong, J.J., Kuo, L.W., Hsu, J.Y., Hung, J.H., 2008. Core-log integration studies in hole-A of Taiwan Chelungpu-fault Drilling Project. Geophys. J. Int. 174, 949–965.

Yabe, Y., Song, S.R., Wang, C.Y., 2008. In-situ stress at the northern portion of the Chelungpu fault, Taiwan, estimated on boring cores recovered from a 2-km-deep hole of TCDP. Earth Planets Space 60, 809–819.

Yeng, K.T., 2000. The residual strength of Chin-Shui shale in relation to the slop stability of Tsao-Ling Mater Thesis Department of Civil Engineering, National Taiwan University, Taipei.

Yue, L.F., Suppe, J., 2014. Regional pore-fluid pressures in the active western Taiwan thrust belt: a test of the classic Hubbert–Rubey fault — weakening hypothesis. J. Struct. Geol. 69, 493–518.

Yuan, X.P., Leroy, Y.M., Maillot, B., 2015. Tectonic and gravity extensional collapses in overpressured cohesive and frictional wedges. J. Geophys. Res. 120, 1833–1854. http://dx.doi.org/10.1002/2014JB011612.

Zhao, W.L., Davis, D.M., Dahlen, F.A., Suppe, J., 1986. Origin of convex accretionary wedges: evidence from Barbados. J. Geophys. Res. 91 (B10), 10246–10258.

Please cite this article as: Yang, C.-M., et al., Non-linear critical taper model and determination of accretionary wedge strength, Tectonophysics (2016), http://dx.doi.org/10.1016/j.tecto.2016.04.026